OPEN ACCESS
JOURNAL OF ADVANCED DIELECTRICS
Vol. 13, No. 5 (2023) 2350015 (7 pages)

DOI: 10.1142/S2010135X23500157

Photocatalytic water splitting kinetics of CMV model

J. H. Hu and C. L. Wang*
School of Physics, Shandong University, Jinan 250100, P. R. China
*wangcl@sdu.edu.cn

Received 14 April 2023; Revised 27 April 2023; Accepted 6 May 2023; Published 31 May 2023

The photocatalytic water splitting kinetics has been analyzed in this paper. The experimental data are taken from the published works and fitted with different theoretical models. From the results, we find that the photocatalytic kinetics of water splitting can be described by Capelas–Mainardi–Vaz (CMV) model very well. This suggests that the water splitting kinetics can be regarded as a fractional first-order kinetics of the chemical reaction. Also, we notice that photocatalytic water splitting is not always completely a monotone kinetics process.

Keywords: Photocatalytic kinetics; water splitting; CMV model; fractional calculus.

1. Introduction

Photocatalytic water splitting is an attractive catalytic process in the formation of hydrogen and oxygen as energy carrier and many materials such as oxide, oxynitride and nitride have been studied.[1–5] Most of the research works have focused on the fundamental aspects of the process, i.e., on optimizing the band structures, improving charge separation and transfer and reducing cost and toxicity.[6,7] Relatively less attention has been focused on the chemical reaction kinetics of the photocatalytic processes. The accurate description of photocatalytic water splitting requires comprehensive mathematical models incorporating both its kinetics and irradiation mechanisms.[8–11] Since these models are usually complex, their careful validation against experimental data is imperative. In the last few years, we have found that chemical reaction kinetics of catalytic degradation process can be well described by Cole–Cole (CC), Cole–Davidson (CD), Havriliak–Negami (HN) and Jurlewicz–Weron–Stanislavsky (JWS) model in time domain.[12–15] All these models can be integrated into a unified expression by Prabhakar fractional calculus.[16] Although these kinetic models are initially proposed for understanding dielectric relaxation process, they have been transplanted for studying chemical reaction kinetics very successfully. Apart from the above models, there are Kohlrausch–Williams–Watts (KWW) model, Capelas–Mainardi–Vaz (CMV) model and the excess wing model for the dielectric relaxations. KWW model is based on stretched exponential function in the time domain. This model was first introduced by Kohlrausch to describe the discharge relaxation phenomenon in Leiden jar capacitors and later was rediscovered by Williams and Watt to describe nonsymmetric dielectric loss curves showing intermediate shapes between the CC and CD models.[17] A novel measurement method of dielectric permittivity has been developed that could extract information for a better understanding of microscopic models of the relaxation process.[18] In a recent paper by CMV, a transcendental function as relaxation function has been proposed,[19] which is known as Kilbas–Saigo function. CMV model is based on Kilbas–Saigo function and is a mathematical bridge between CC model and KWW model.

To find out the kinetics type in the photocatalytic water splitting process, we have adopted different kinetics models, which are presented in Ref. 17 by Garrappa, Mainardi and Maione, to be fitted with the experimental data of hydrogen or oxygen production evolution in previously published papers. We notice that the CMV model can be applied to describe the experimental data of the evolution process much better. Hence, in this paper, the CMV model is formulated for the photocatalytic water splitting kinetics and selected fitting results of experimental data with this model are presented and discussed.

2. Model and Method

For the evolution of hydrogen or oxygen production concentration $C(t)$ at time t of a photocatalytic water splitting process, the differential equation of CMV model can be written as follows:[17]

$$ {}_0^C D_t^{\alpha}[C(t)] = \frac{t^{\beta}}{\tau^{\alpha+\beta}}[C_{\infty} - C(t)], \tag{1} $$

where ${}_0^C D_t^{\alpha}$ is the fractional derivative of α-order in sense Caputo type, β is the model parameter, τ is the

*Corresponding author.

characteristic time, C_∞ is the saturated value of concentration $C(t)$ at infinite time. The initial value of concentration is zero, i.e.,

$$C(t)\big|_{t=0} = 0. \tag{2}$$

The solution of differential Eq. (1) with initial condition (2) is as follows:

$$C(t) = C_\infty \left[1 - E_{\alpha,1+\frac{\beta}{\alpha},\frac{\beta}{\alpha}}\left(-\left(\frac{t}{\tau}\right)^{\alpha+\beta}\right)\right]. \tag{3}$$

Here, $E(\cdot)$ is the Kilbas–Saigo function, which is a three-parameter Mittag–Leffler function defined as follows:[19]

$$E_{\alpha,m,l}(z) = \sum_{n=0}^{\infty} c_n z^n, \quad c_n = \prod_{i=0}^{n-1} \frac{\Gamma(\alpha(i\cdot m + l) + 1)}{\Gamma(\alpha(i\cdot m + l + 1) + 1)}, \tag{4}$$

where $\Gamma(\cdot)$ denotes the Euler's gamma function. When $\alpha = 1$, this model reduces to KWW model of the stretched exponential functional form as follows:

$$C(t) = C_\infty \left(1 - e^{-(t/\tau)^\beta + 1}\right). \tag{5}$$

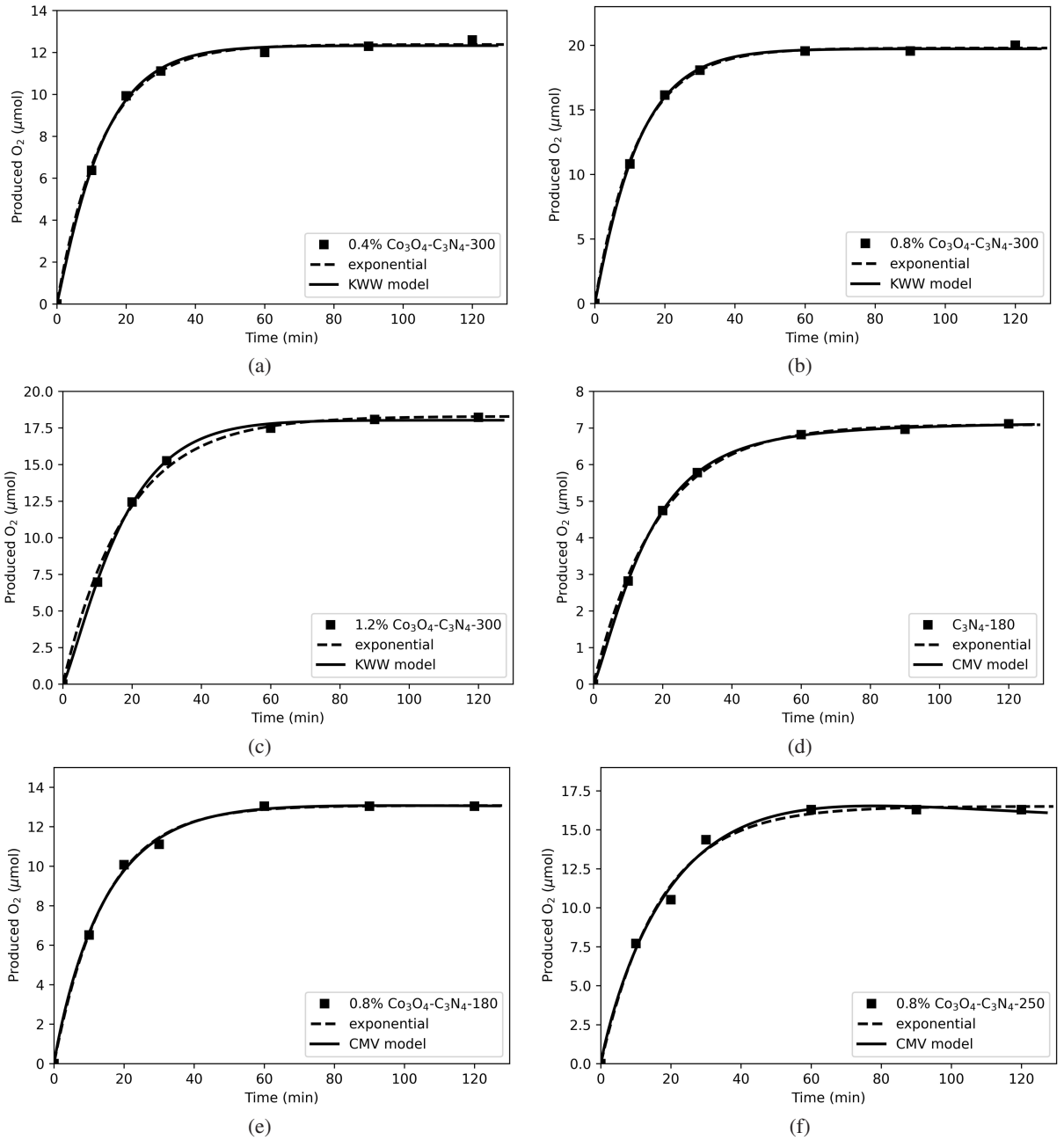

Fig. 1. Oxygen production evolution curves. Solid lines for CMV model, dashed lines for exponential function fitting and solid square symbols for experimental data[20] with different amounts of Co_3O_4 under different annealing temperatures.

When $\beta = 0$, Eq. (3) reduces to the CC model and can be expressed by one-parameter Mittag–Leffler function as follows:

$$C(t) = C_\infty \left(1 - E_\alpha\left(-(t/\tau)^\alpha\right)\right). \quad (6)$$

When both $\alpha = 1$ and $\beta = 0$ happen, the CMV model is reduced to the exponential function, which belongs to a standard integer first-order chemical reaction kinetics, i.e.,

$$C(t) = C_\infty (1 - e^{-t/\tau}). \quad (7)$$

The complete monotone condition for solution in Eq. (3) requires

$$0 < \alpha \le 1, \quad -\alpha < \beta \le 1 - \alpha\,. \quad (8)$$

The complete monotone condition means that the function and its derivatives are all monotonic functions. This suggests that hydrogen or oxygen production concentration changes with time monotonically, and their generation rate changes with time monotonically either, and so on so forth.

Fitting of CMV model in Eq. (3) with the experimental data has been done using the least square method. The exponential model of Eq. (7) is also fitted for comparison. Model parameters α and β, as well as characteristic time τ and saturated concentration C_∞ are returned from the fittings. The coefficient of determination R^2 is also calculated for checking validation of the models.

Since the solution in Eq. (3) is not a linear function, the fitting approach with the experimental data is similar to our previous works.[12–15] All the numerical calculations have been done in Python code. Fitting results with reasonable values of model parameters are kept and presented in this paper. The first experimental dataset is chosen from monodisperse Co_3O_4 quantum dots on porous carbon (PC) nitride nanosheets for enhanced visible-light-driven water oxidation.[20] Second experimental dataset is from bio-waste-derived few-layered graphene (FLG)/$SrTiO_3$/PAN as an efficient photocatalytic system for water splitting.[21] Third dataset is about catalytic hydrogen evolution of $NaBH_4$ hydrolysis by cobalt nanoparticles supported on bagasse-derived PC.[22]

3. Results and Discussions

Fitting curves of the oxygen production evolution from monodisperse Co_3O_4 quantum dots on PC nitride nanosheets under irradiation of visible light with different annealing temperatures are shown in Fig. 1. The corresponding fitting parameters are listed in Table 1. Experimental data are denoted as solid squares in Fig. 1, dashed lines stand for the fitting with exponential function model of Eq. (7) and solid lines are for the CMV model of Eq. (3). The notation of the catalyst name is the same as of that in the original paper,[20] i.e., the percentage numbers mean the amount of Co_3O_4, and the last number stands for the annealing temperature in centigrade. The last column in Table 1 specifies the fitting model,

Table 1. Fitting parameters with experimental data of oxygen production by Co_3O_4 quantum dots on C_3N_4 nanosheets.[20]

Catalyst	C_∞	τ (min)	α	$\beta + 1$	R^2	Model
0.4% Co_3O_4-C_3N_4-300	12.38	13.17	1.00	1.00	0.9982	Expo
	12.32	12.32	1.00	1.08	0.9985	KWW
0.8% Co_3O_4-C_3N_4-300	19.79	12.28	1.00	1.00	0.9994	Expo
	19.73	11.70	1.00	1.06	0.9995	KWW
1.2% Co_3O_4-C_3N_4-300	18.30	18.27	1.00	1.00	0.9968	Expo
	18.03	15.23	1.00	1.21	0.9994	KWW
C_3N_4-180	7.09	18.51	1.00	1.00	0.9991	Expo
	7.22	16.22	0.84	1.20	0.9999	CMV
0.8% Co_3O_4-C_3N_4-180	13.07	14.38	1.00	1.00	0.9985	Expo
	12.96	15.11	1.04	0.95	0.9985	CMV
0.8% Co_3O_4-C_3N_4-250	16.51	16.92	1.00	1.00	0.9931	Expo
	15.15	17.23	1.22	0.92	0.9943	CMV

with Expo for the exponential model of Eq. (7) and KWW of Eq. (6) and CMV of Eq. (5). It is obvious either from the diagrams in Fig. 1 and the coefficient of determination of R^2 in Table 1 that there is only a marginal difference between the CMV fitting and the exponential function model for all the catalysts. This implies that the water splitting process with Co_3O_4 quantum dots on PC nitride nanosheets can follow the first-order kinetics very well.

The catalyst with 0.8% Co_3O_4 quantum dots annealing at 300°C shows the best performance, i.e., with the largest saturated product of oxygen C_∞ and the shortest characteristic time τ, see the second row as listed in Table 1. This implies that this catalyst can produce a large amount of oxygen in a short time. For all samples annealing at 300°C, they follow KWW model slightly better, as shown in Figs. 1(a)–1(c) and the parameters listed in the first three rows of Table 1. For catalysts annealing at temperatures different from 300°C, their kinetic behavior follows the CMV model slightly better, as shown in Figs. 1(d)–1(f) and parameters listed in the last three rows of Table 1. However, we also notice that model parameters α and β do not satisfy the monotone condition of Eq. (8) for all the catalysts listed in Table 1. That means that these kinetic processes are not monotonic, either the oxygen production amount or the production rate do not change with time monotonically. This behavior can be seen quite obviously in Fig. 1(f) of catalyst 0.8%Co_3O_4-C_3N_4-250, the oxygen production begins to decrease at a long time limit.

Fitting curves of photocatalytic activities of composites based on synthesized $SrTiO_3$ and bio-waste-derived FLG and commercial graphene oxide (GO)[21] are shown in Fig. 2. The bio-waste-derived FLG are synthesized from rice husk (RH) and walnut shells (WS). Polyacrylonitrile (PAN) is served as the nuclei for carbon structure. The catalyst name is denoted as c-$SrTiO_3$/PAN/x-FLG, here c-means calcined, and *x*-stands for GO, RH or WS. The hydrogen and oxygen production evolution dependence on the irradiation time is fitted, the

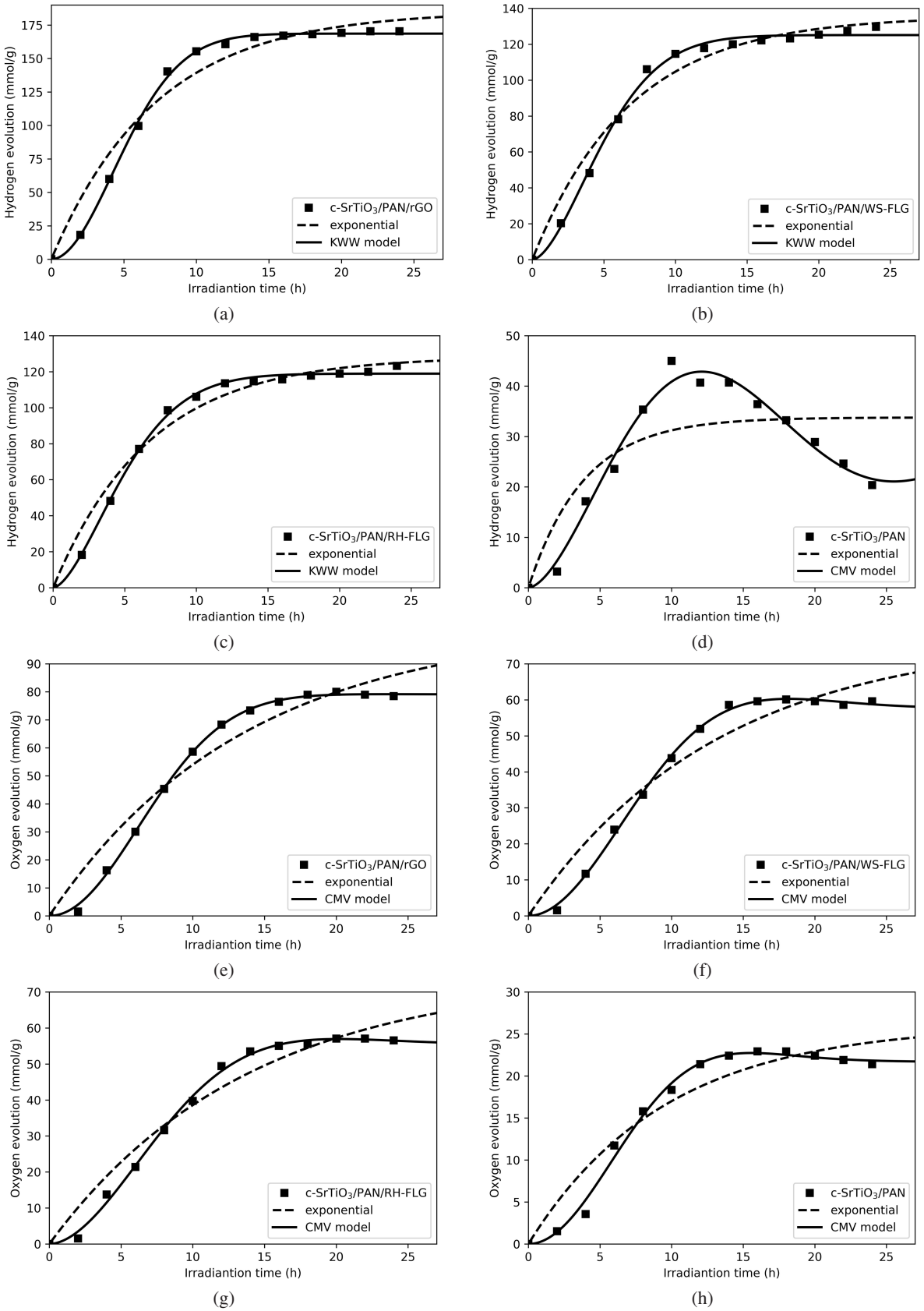

Fig. 2. Hydrogen and oxygen production evolution curves. Solid lines for CMV model, dashed lines for exponential function fitting and solid square symbols for experimental data with bio-waste-derived FLG/$SrTiO_3$/PAN.[21]

Table 2. Fitting parameters with experimental data of bio-waste-derived FLG/$SrTiO_3$/PAN.[21]

Catalyst	C_∞	τ (h)	α	$\beta+1$	R^2	Model
H_2: c-$SrTiO_3$/ PAN/GO	185.47	7.19	1.00	1.00	0.9580	Expo
	168.62	6.16	1.00	1.93	0.9989	KWW
H_2: c-$SrTiO_3$/ PAN/ WS-FLG	135.63	6.76	1.00	1.00	0.9716	Expo
	125.11	4.34	1.00	1.69	0.9963	KWW
H_2: c-$SrTiO_3$/ PAN/ RH-FLG	128.37	6.67	1.00	1.00	0.9754	Expo
	118.92	4.37	1.00	1.63	0.9979	KWW
H_2: c-$SrTiO_3$/ PAN	33.78	3.87	1.00	1.00	0.6655	Expo
	28.93	1.86	1.84	1.67	0.9823	CMV
O_2: c-$SrTiO_3$/ PAN/GO	103.70	13.60	1.00	1.00	0.9527	Expo
	79.01	6.04	1.02	2.02	0.9991	CMV
O_2: c-$SrTiO_3$/ PAN/ WS-FLG	74.62	13.74	1.00	1.00	0.9574	Expo
	54.93	5.67	1.16	1.83	0.9974	CMV
O_2: c-$SrTiO_3$/ PAN/ RH-FLG	77.49	13.12	1.00	1.00	0.9447	Expo
	57.18	5.28	1.21	1.95	0.9986	CMV
O_2: c-$SrTiO_3$/ PAN	26.09	9.48	1.00	1.00	0.9242	Expo
	21.55	4.58	1.22	2.00	0.9932	CMV

catalyst name is labeled in each diagram of Fig. 2. The fitting parameters are listed in Table 2, the first four rows are for the hydrogen generation and the last four rows are for the oxygen generation. We have noticed that the notation of curves on the hydrogen and oxygen evolution could be labeled inappropriately in the original paper, but the discussions are addressed appropriately.[21]

It can be seen quite easily from Fig. 2 that the production evolution of hydrogen and oxygen is deviated from the standard exponential function model as shown in the dashed lines. The coefficients of determination R^2 are all over 0.99% for fitting with the CVM model or KWW model, except in the only case of hydrogen evolution by c-$SrTiO_3$/PAN as shown in Fig. 2(d). Also, we notice that all the oxygen evolution follows the CMV model quite well. But the hydrogen evolution follows much better with the KWW model, which is also a special case of the CMV model.

The catalyst with commercial graphene oxide has the best photocatalytic water splitting performance, as shown in Fig. 2(a) for hydrogen generation and Fig. 2(e) for oxygen generation. Catalysts with bio-waste-derived few-layer graphene, i.e., with RHs and WSs, also show a very good performance, this can be seen from Figs. 2(b) and 2(d) for hydrogen generation, and Figs. 2(f) and 2(g) for oxygen generation. By comparison with catalyst of no graphene decorations, i.e., the case shown in Figs. 2(d) and 2(e) for hydrogen and oxygen, respectively, water splitting efficiency is much enhanced by the decoration of RHs and WSs. Again, we notice that model parameters in the water splitting process do not satisfy the complete monotone conditions. The non-monotone behavior is quite strong in Figs. 2(d), 2(f) and 2(h), respectively.

Fitting curves of photocatalytic hydrogen production evolution of sodium borohydride ($NaBH_4$) hydrolysis by cobalt nanoparticles supported on bagasse-derived PC[22] is shown in Fig. 3. Bagasse is used as raw material for the preparation of PC, then PC to load Co nanoparticles (denoted as Co@xPC) for $NaBH_4$ hydrolysis. Here, x in Co@xPC means the amounts of PC, *f.i.*, Co@150PC stands 150 mg of PC are added. The influence of the addition of PC on the catalytic performance of Co has been fitted and shown in Figs. 3(a)–3(d), with the first diagram for the case of no PC addition. The fitting parameters are listed in the first four rows of Table 3. The hydrogen production evolution of $NaBH_4$ catalyzed by different amounts of Co@150PC, i.e., 0.05, 0.10, 0.15 and 0.20 g, respectively, has been fitted and shown in Figs. 3(e)–3(h). The fitting parameters are listed in the last four rows of Table 3 correspondingly.

It can be seen from the diagrams in Fig. 3 and the parameters listed in Table 3 that the CMV model or KWW model can be fitted much better than the exponential function model. It is interesting to note that only the production evolution of cobalt particle catalyst without PC follows the KWW model, as shown in Fig. 3(a) and the first row in Table 3. For all other catalysts with the addition of PC, their behavior follows the CMV model as shown in Figs. 3(b)–3(h) and rows 2–8 in Table 3. Once again, we notice the nonmonotonic behavior of the photocatalytic water splitting process, and it is more obvious in the cases as shown in Figs. 3(d), 3(g) and 3(h).

The best performance catalyst for water splitting is still a cobalt particle catalyst without PC, see the first row in Table 3. It has the largest saturated value C_∞ and a relative longer characteristic time τ. That means it produces much more hydrogen, but takes much longer time than other catalysts. From the CMV model, we know that catalyst Co@100PC produces more hydrogen as it has a larger saturated value than other catalysts with PC additions. Catalyst Co@150PC produces hydrogen more quickly since it has a shorter characteristic time than other catalysts with PC additions. However, the behavior is different from the fitting results of the exponential function model. For $NaBH_4$ catalyzed by different amounts of Co@150PC, the saturated value increases with the amounts of Co@150PC. For the characteristic time, 0.05 g Co@150PC has the shortest value, then 0.15 g Co@150PC, the longest characteristic time happens with 0.20 g Co@150PC. By comparison with the exponential function model, the CMV model predicts smaller saturated value and shorter characteristic time for all catalysts.

4. Summary

Chemical reaction kinetics of the CMV model has been observed in catalysts for photocatalytic water splitting processes. Our fitting results suggest that water splitting kinetics can be regarded as a fractional first-order chemical reaction kinetics. Also, we notice that the production evolution is not

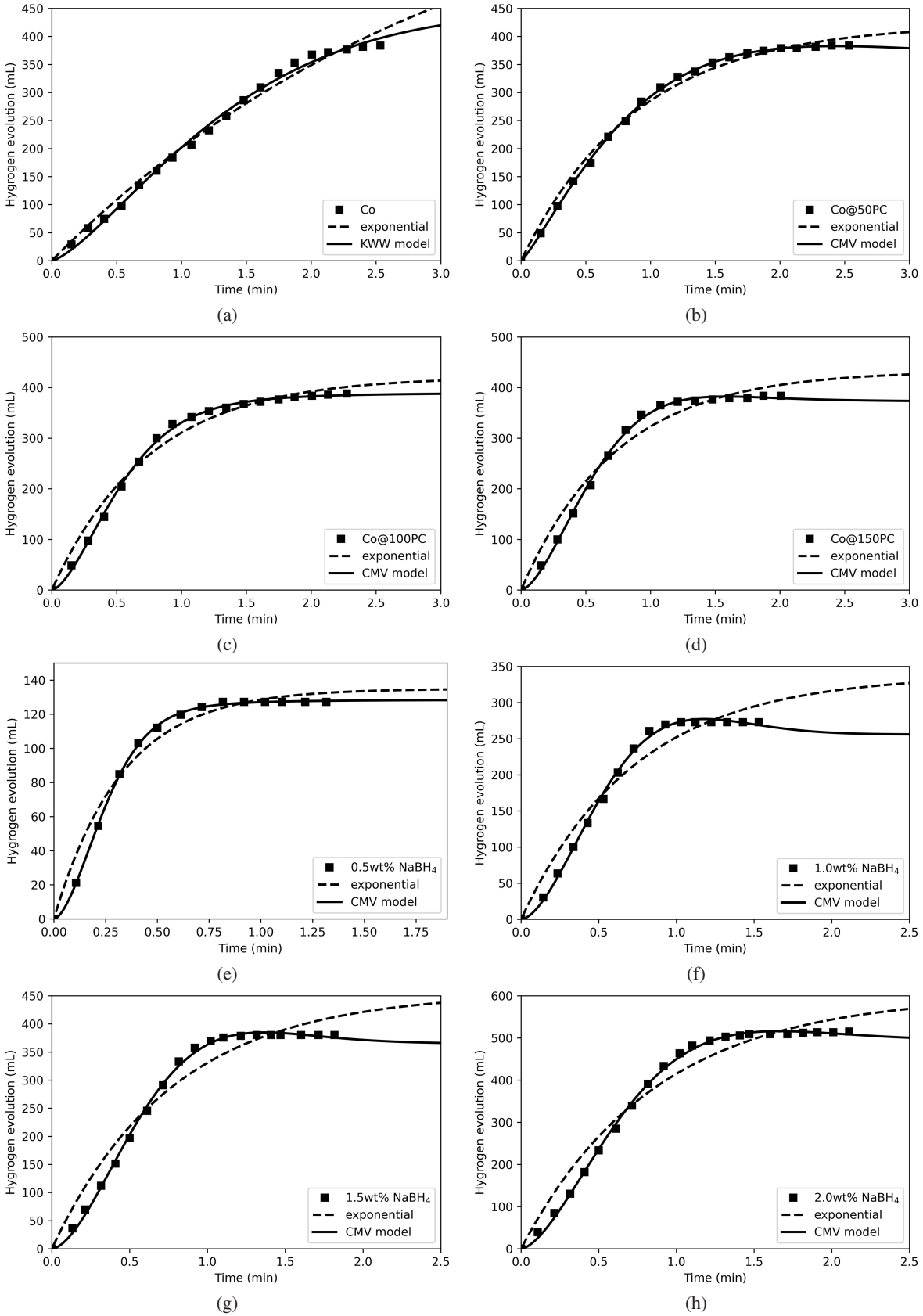

Fig. 3. Solid lines for CMV model, dashed lines for exponential function, solids square symbols for experimental data cobalt nanoparticles on bagasse-derived PC.[22]

Table 3. Fitting parameters with experimental data of cobalt nanoparticles on bagasse-derived PC.[22]

Catalyst	C_∞	τ (min)	α	$\beta+1$	R^2	Model
Co	748.65	3.19	1.00	1.00	0.9903	Expo
	451.11	1.16	1.00	1.37	0.9960	KWW
Co@50PC	422.27	0.89	1.00	1.00	0.9923	Expo
	355.11	0.56	1.23	1.20	0.9995	CMV
Co@100PC	421.51	0.75	1.00	1.00	0.9801	Expo
	391.26	0.50	0.89	1.59	0.9987	CMV
Co@150PC	433.21	0.73	1.00	1.00	0.9688	Expo
	371.04	0.41	1.13	1.60	0.9982	CMV
0.05 g Co@150PC	26.09	9.48	1.00	1.00	0.9242	Expo
	21.55	4.58	1.22	2.00	0.9932	CMV
0.10 g Co@150PC	74.62	13.74	1.00	1.00	0.9574	Expo
	54.93	5.67	1.16	1.83	0.9974	CMV
0.15 g Co@150PC	77.49	13.12	1.00	1.00	0.9447	Expo
	57.18	5.28	1.21	1.95	0.9986	CMV
0.20 g Co@150PC	103.70	13.60	1.00	1.00	0.9527	Expo
	79.01	6.04	1.02	2.02	0.9991	CMV

a completely monotone behavior. We believe that this is the first time that this theoretical model is validated by experimental evidence.

Acknowledgment

This work is supported by the National Natural Science Foundation of China (51672159, 51501105 and 51611540342).

References

[1]Y. Y. Kim, M. Watanabe, J. Matsuda, J. T. Song, A. Takagaki, A. Staykov and T. Ishihara, Tensile strain for band engineering of $SrTiO_3$ for increasing photocatalytic activity to water splitting, *Appl. Catal. B. Environ*. **278**, 119292 (2020).

[2]K. Maeda, Photocatalytic water splitting using semiconductor particles: History and recent de-velopments, *J. Photochem. Photobiol. C Photochem. Rev.* **12**, 237 (2011).

[3]M. Ni, M. K. H. Leung, D. Y. C. Leung and K. Sumathy, A review and recent developments in photocatalytic water splitting using TiO_2 for hydrogen production, *Renew. Sustain. Energy Rev.* **11**, 401 (2007).

[4]F. E. Osterloh, Inorganic nanostructures for photo-electrochemical and photocatalytic water splitting, *Chem. Soc. Rev.* **42**, 2294 (2013).

[5]A. Kudo and Y. Miseki, Heterogeneous photocatalyst materials for water splitting, *Chem. Soc. Rev.* **38**, 253 (2009).

[6]M. Edelmannova, M. M. Ballari, M. Pribyl and K. Kocí, Experimental and modelling studies on the photocatalytic generation of hydrogen during water splitting over a commercial TiO_2 photocatalyst P25, *Energy Convers. Manag.* **245**, 114582 (2021).

[7]X. Li, J. G. Yu, J. X. Low, Y. P. Fang, J. Xiao and X. B. Chen, Engineering heterogeneous semiconductors for solar water splitting, *J. Mater. Chem. A* **3**, 2485 (2015).

[8]E. Hojaji, M. Valant and A.-K. Axelsson, Comprehensive adsorption and irradiation modelling of LED driven photoreactor for H_2 production, *Chem. Eng. J.* **406**, 126860 (2021).

[9]J. Marugan, R. Grieken, A. E. Cassano and O. M. Alfano, Intrinsic kinetic modeling with explicit radiation absorption effects of the photocatalytic oxidation of cyanide with TiO_2 and silica-supported TiO_2 suspensions, *Appl. Catal. B. Environ*. **85**, 48 (2008).

[10]J. Marugan, R. Grieken, A. E. Cassano and O. M. Alfano, Quantum efficiency of cyanide photo-oxidation with TiO_2/SiO_2 catalysts: Multivariate analysis by experimental design, *Catal. Today* **129**, 143 (2007).

[11]E. Lilov, V. Lilova, S. Nedev, S. Kozhukharov and C. Girginov, Model for photodegradation with a modified rate constant. Part 2: Model description, *J. Chem. Technol. Metall.* **57**, 1175 (2014).

[12]C. L. Wang, Fractional kinetics of photocatalytic degradation, *J. Adv. Dielectr*. **8**, 1850034 (2018).

[13]C. L. Wang, Photocatalytic degradation as Davidson-Cole relaxation in time domain, *J. Adv. Dielectr.* **9**, 1950006 (2019).

[14]C. L. Wang, Piezo-catalytic degradation of Havriliak-Negami type, *J. Adv. Dielectr.* **9**, 1950021 (2019).

[15]C. L. Wang, Photo-catalytic degradations of JWS kinetics, *J. Adv. Dielectr.* **11**, 2150029 (2021).

[16]A. Giusti, I. Colombaro, R. Garra, R. Garrappa, F. Polito, M. Popolizio and F. Mainardi, A practical guide to Prabhakar fractional calculus, *Fract. Calc. Appl. Anal*. **23**, 9 (2020).

[17]R. Garrappa, F. Mainardi and G. Maione, Models of dielectric relaxation based on completely monotone functions, *Fract. Calc. Appl. Anal.* **19**, 1105 (2016).

[18]J. L. Swantek, T. D'Esposito, J. Brannum and F. V. Kowalski, Dielectric relaxation affected by a monotonically decreasing driving force: An energy perspective, *J. Appl. Phys.* **130**, 154101 (2021).

[19]E. Capelas de Oliveira, F. Mainardi, Jr. and J. Vaz, Fractional models of anomalous relaxation based on the Kilbas and Saigo function, *Meccanica* **49**, 2049 (2014).

[20]H. Y. Zhang, W. J. Tian, L. Zhou, H. Q. Sun, M. Tade and S. B. Wang, Monodisperse Co_3O_4 quantum dots on porous carbon nitride nanosheets for enhanced visible-light-driven water oxidation, *Appl. Catal. B Environ.* **223**, 2 (2018).

[21]C. Daulbayev, F. Sultanov, A. V. Korobeinyk, M. Yeleuov, S. Azat, B. Bakbolat, A. Umirzakov and Z. Mansurov, Bio-waste-derived few-layered graphene /$SrTiO_3$/PAN as efficient photocatalytic system for water splitting, *Appl. Surf. Sci.* **549**, 149176 (2021).

[22]E. Karamian and S. Sharifnia, Catalytic hydrogen evolution of $NaBH_4$ hydrolysis by cobalt nanoparticles supported on bagasse-derived porous from carbon, *Nanomaterials* **11**, 3259 (2021).